Inorganic Chemistry

pubs.acs.org/IC

Article

Facile Light-Induced Transformation of $[Ru^{II}(bpy)_2(bpyNO)]^{2+}$ to $[Ru^{II}(bpy)_3]^{2+}$

Alireza Karbakhsh Ravari, Yuliana Pineda-Galvan, Alexander Huynh, Roman Ezhov, and Yulia Pushkar*

Cite This: https://dx.doi.org/10.1021/acs.inorgchem.0c01446

Read Online

ACCESS | Metrics & More | Article Recommendations | Supporting Information

ABSTRACT: Ru-based coordination compounds have important applications as photosensitizers and catalysts. $[Ru^{II}(bpy)_2(bpyNO)]^{2+}$ (bpy = 2,2′-bipyridine and bpyNO = 2,2′-bipyridine-*N*-oxide) was reported to be extremely light-sensitive, but its light-induced transformation pathways have not been analyzed. Here, we elucidated a mechanism of the light-induced transformation of $[Ru^{II}(bpy)_2(bpyNO)]^{2+}$ using UV−vis, EPR, resonance Raman, and NMR spectroscopic techniques. The spectroscopic analysis was augmented with the DFT calculations. We concluded that upon 530−650 nm light excitation, $^3[Ru^{III}(bpyNO^{-\bullet})(bpy)_2]^{2+}$ is formed similarly to the $^3[Ru^{III}(bpy^{-\bullet})(bpy)_2]^{2+}$ light-induced state of the well-known photosensitizer $[Ru^{II}(bpy)_3]^{2+}$. An electron localization on the bpyNO ligand was confirmed by obtaining a unique EPR signal of reduced $[Ru^{II}(bpy)_2(bpyNO^{-\bullet})]^{+}$ (g_{xx} = 2.02, g_{yy} = 1.99, and g_{zz} = 1.87 and ^{14}N hfs A_{xx} = 12 G, A_{yy} = 34 G, and A_{zz} = 11 G). $^3[Ru^{III}(bpyNO^{-\bullet})(bpy)_2]^{2+}$ may evolve via breaking of the Ru−O−N fragment at two different positions resulting in $[Ru^{IV}{=}O(bpy)_2(bpy_{out})]^{2+}$ for breakage at the O-l-N bond and $[Ru^{II}(H_2O)(bpy)_2(bpyNO_{out})]^{2+}$ for breakage at the Ru-l-O bond. These pathways were found to have comparable ΔG. A reduction of $[Ru^{IV}{=}O(bpy)_2(bpy_{out})]^{2+}$ may result in water elimination and formation of $[Ru^{II}(bpy)_3]^{2+}$. The expected intermediates, $[Ru^{III}(bpy)_2(bpyNO)]^{3+}$ and $[Ru^{III}(bpy)_3]^{3+}$, were detected by EPR. In addition, a new signal with g_{xx} = 2.38, g_{yy} = 2.10, and g_{zz} = 1.85 was observed and tentatively assigned to a complex with the dissociated ligand, such as $[Ru^{III}(H_2O)(bpy)_2(bpyNO_{out})]^{3+}$. The spectroscopic signatures of $[Ru^{IV}{=}O(bpy)_2(bpy_{out})]^{2+}$ were not observed, although DFT analysis and $[Ru^{II}(bpy)_3]^{2+}$ formation suggest this intermediate. Thus, $[Ru^{II}(bpy)_2(bpyNO)]^{2+}$ has potential as a light-induced oxidizer.

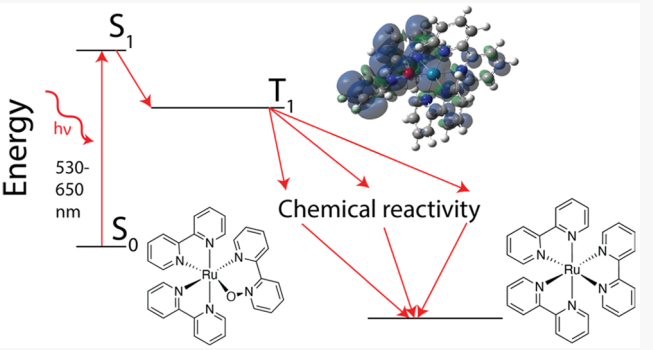

INTRODUCTION

Ru based coordination compounds were developed as catalysts,[1−5] photosensitizers,[6,7] and anticancer drugs.[8,9] Multiple Ru-based polypyridine complexes draw considerable attention as they are easily modifiable, stable catalysts, and sensitizers in processes with harsh reaction conditions such as oxidation reactions.[10−12] Their analogs, Ru coordination compounds with polypyridyl *N*-oxides, were noted in multiple Ru-based catalytic systems under the conditions of water oxidation.[13−16] Polypyridyl *N*-oxides are reactive compounds with applications in chemical synthesis, catalysis, and drug design.[17,18] Their combination with the photoactive Ru catalytic centers may result in novel, unusual properties particularly suitable for the oxidation reactions.[19,20] Out of these considerations, we studied the photochemical transformations of $[Ru^{II}(bpy)_2(bpyNO)]^{2+}$ (**1-NO**), a compound with pronounced light sensitivity.[15,21] Its structural predecessor, $[Ru(bpy)_3]^{2+}$ (**1**), is widely known as a photosensitizer with well-understood photochemistry and has wide-ranging applications in a photoredox catalysis.[22−24] The analogs of this compound are also used in dye-sensitized solar cells.[25] This compound appears as a single product of (**1-NO**) irradiation. Previously, (**1-NO**) behavior was analyzed in oxidation.[15] For instance, the oxidation of (**1-NO**) in the dark with Ce(IV) ammonium nitrate (Ce^{IV}) resulted in a majority conversion to $[Ru^{III}(bpy)_2(bpyNO)]^{3+}$. A minority, assigned to an open form, $[Ru^{II}(H_2O)(bpy)_2(bpyNO_{out})]^{2+}$, is capable of O−O bond formation and O_2 evolution via the proposed $[Ru^{IV}{=}O(bpy)_2(bpyNO^{+\bullet}{}_{out})]^{3+}$ intermediate.[15] After oxidation with Ce^{IV} in the dark, the $Ru^{IV}{=}O$ moiety vibration was detected at ~799 cm^{-1}.[15] Here, we describe the behavior of (**1-NO**) under the illumination with visible light (530−650 nm). A relatively short (5−30 min) exposure of (**1-NO**) solution in water or acetonitrile to ambient light resulted in irreversible changes in its UV−vis spectrum. We were able to characterize a final

Received: May 17, 2020

product of the light-induced transformation as (**1**). We propose that light-induced $^3[Ru^{III}(bpyNO^{-\bullet})(bpy)_2]^{2+}$ is capable of dissociating the *N*-oxide group with formation of the intermediate $[Ru^{IV}{=}O(bpy)_2(bpy_{out})]^{2+}$, which later reduces to (**1**) and water.

EXPERIMENTAL SECTION

Synthesis. Complex (**1-NO**) was prepared using the published procedure.[15]

Sample Illumination. All samples were exposed to LED lamps with 530 nm (10 W), 650 nm (10 W), and 760 nm (15 W). The spectrum of each LED was measured, and the fwhm of each LED was less than 15 nm. Each sample was exposed to intense LED light (15 cm away from the light source) for 30 min in a heat bath to keep the temperature constant (room temperature) during the experiment. No change in the neutral pH was observed while irradiating samples in water.

Raman Spectroscopy. A HeCd CW laser (442 nm and ∼15 mW) was employed for the resonance Raman. The measurement was conducted at room temperature; hence, the sample was in liquid form. To minimize background, measurements were done on a hanging drop partially extruded from a syringe prefilled with sample solution. The sample area directly exposed to the laser was a circle with a diameter of ∼0.5 mm. The laser beam was focused on the sample with fused silica lens with 10 cm focal length. The (Raman signal) light-collecting system consisted of two fused silica lenses: the first lens was the same lens which focused the laser beam on the sample, and the second lens focused the collected signal on the monochromator slit. The slit width during the measurement was 70 μm. A Semrock edge pass filter prevented Rayleigh scattering to get into the monochromator. A holographic grating with 1800 l/mm was used to disperse the Raman signal onto the detector. An iDus 420 Andor camera was used.

EPR Spectroscopy. A 200 μL aliquot of sample with 1 mM concentration in 0.1 M HNO_3 was added to EPR tubes and frozen in liquid nitrogen (in less than 30 s). Low-temperature (20 K using ColdEdge closed cycle cryostat) X-band EPR spectra were recorded with a Bruker EMX X-band spectrometer and X-Band CW microwave bridge. For EPR signal quantitation, the standard EPR sample tubes were filled with the samples through all of the resonator space. The signal intensities were measured on the same day and in the same conditions to allow direct comparison of the signal intensities. For the spectrum simulation, SimFonia software from Bruker was used.

UV−Vis Absorption Spectroscopy. A Cary 300 UV−vis spectrometer was used for the absorption measurements. The sample was held in a quartz cuvette with 1 mm light path at room temperature.

Oxygen-evolution measurement. Oxygen-evolution measurements of 1 mM and 4 mM $Ru(bpy)_2(bpyNO)(PF_6)_2$ water solutions were performed under irradiation with visible light. In a typical experiment, 0.5 mL of (**1-NO**) solution was added to an Oxygraph System (Hansatech Instruments, Ltd.) chamber and constantly stirred, followed by illumination with a 150 W halogen lamp, covering the entire visible range, for 30 min. Oxygen concentration was recorded as a function of time. Calibration was performed by measuring a signal in oxygen-saturated deionized water (284 μM/L at 20 °C), followed by an addition of the oxygen-depleted reagent (sodium dithionite).

DFT. Gaussian16 software with the B3LYP exchange-correlation (XC) functional was used for DFT calculations. The 6-31G* basis was set for all organic atoms (C, O, N, and H), and the all-electron DGDZVP basis was set for the Ru atom. To model water solvation, the CPCM polarizable conductor model was used. The value of the reference potential (NHE) was assigned to 4.44 V, and the free energy of a solvated proton was set to −11.64 V.

NMR. NMR spectra were recorded on a Bruker AV-III-HD-400 400 MHz spectrometer, and chemical shifts were referenced to solvent residual peaks. ^{1}H NMR of (**1-NO**) (400 MHz, CD_3CN) σ/ppm: 8.98 (d, 1H), 8.70 (d, 1H), 8.57−8.50 (m, 2 H), 8.38 (dd, 2H), 8.25 (t, 1H), 8.09−8.05 (m, 4 H), 7.98−7.88 (m, 4 H), 7.84 (d, 1 H), 7.75−7.69 (m, 2 H), 7.48 (d, 1 H), 7.41 (t, 1 H), 7.31−7.26 (m, 2 H), 7.22−7.15 (m, 2 H). ^{1}H NMR of (**1-NO**) (400 MHz, D_2O) σ/ppm: 8.96 (d, 1 H), 8.74 (d, 1 H), 8.60−8.58 (m, 2 H), 8.46−8.42 (m, 2 H), 8.26 (t, 1 H), 8.19 (s, 1 H), 8.15 (s, 1 H), 8.10−8.03 (m, 2 H), 8.01−7.88 (m, 5 H), 7.69 (t, 1 H), 7.55 (d, 1 H), 7.40−7.33 (m, 3 H), 7.26 (t, 1 H), 7.21−7.13 (m, 2 H).

In situ NMR experiments were performed in D_2O (>99.8 atom % D) and CD_3CN (>99.8 atom % D) by irradiation of D_2O and CD_3CN solutions of (**1-NO**) with LEDs at 520 and 659 nm. ^{1}H NMR (400 MHz, D_2O) σ/ppm after irradiation: 8.55 (d, 6 H), 8.05 (t, 6 H), 7.82 (d, 6 H), 7.38 (t, 6 H). ^{1}H NMR (400 MHz, CD_3CN) σ/ppm after irradiation: 8.51 (d, 6 H), 8.07 (t, 6 H), 7.74 (d, 6 H), 7.41 (t, 6 H).

RESULTS

Redox Behavior. In the previous report, we outlined the main spectroscopic and redox properties of $[Ru^{II}(bpy)_2(bpyNO)]^{2+}$ (**1-NO**).[15] (**1-NO**) is EPR-silent with Ru^{2+} in the d^6 electronic configuration, a singlet (S = 0) low-spin state and the neutral ligands. A singlet state allows a convenient investigation of (**1-NO**) by NMR. Upon addition of 1 equiv of an oxidant or reductant, it converts into a S = 1/2 species $[Ru^{III}(bpy)_2(bpyNO)]^{3+}$[15] (will be discussed later in the EPR studies section) and $[Ru^{II}(bpy)_2(bpyNO^{\bullet-})]^{1+}$, correspondingly. An EPR spectrum of the reduced (**1-NO**) (Figure 1) was generated by addition of 1 equiv of sodium

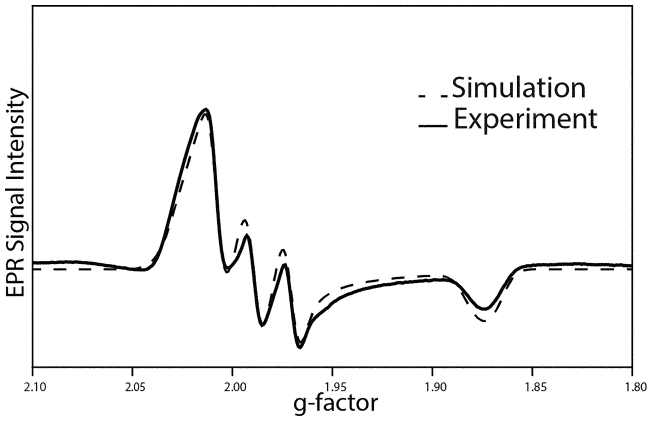

Figure 1. X-band EPR of $[Ru^{II}(bpy)(bpyNO^{\bullet-})]^{1+}$ obtained by (**1-NO**) reduction with ascorbate in water. The measurement was conducted at 20 K, using a modulation amplitude of 10 G and 30 mW of power. Dashed line is the simulated spectrum.

ascorbate (Asc). The EPR spectrum was simulated with g-factors g_{xx} = 2.02, g_{yy} = 1.99, and g_{zz} = 1.87 as well as A_{xx} = 12 G, A_{yy} = 34 G, and A_{zz} = 11 G. The signal shape and g-factor of reduced (**1**), $[Ru^{II}(bpy)_2(bpy^{\bullet-})]^{1+}$, were reported previously[26] and are significantly different from those of reduced (**1-NO**) in Figure 1. Asc is a mild reductant with an estimated redox potential of ca. −0.3 V.[27] Earlier, it was found that the *N*-oxides of pyridine origin were difficult to reduce in the aprotic solvents.[28] An interaction of a polypyridine *N*-oxide ligand with the Ru^{II} center is likely to lower the reduction potential. The redox potential for the reduction of (**1-NO**) was measured as −0.4 V vs NHE by cyclic voltammetry in acetonitrile solution with 0.1 M Et_4NClO_4 as an electrolyte.

Table 1 shows the DFT-estimated redox potentials. A one-electron oxidation allows conversion of the Ru center to a paramagnetic $[Ru^{III}(bpy)_2(bpyNO)]^{3+}$, while further oxidation

https://dx.doi.org/10.1021/acs.inorgchem.0c01446
Inorg. Chem. XXXX, XXX, XXX−XXX

Table 1. Redox Properties of $[Ru^{II}(bpy)_2(bpyNO)]^{2+}$ and $[Ru^{II}(bpy)_3]^{2+}$ from DFT Analysis[a]

	$E°$/V
$Asc^- \rightarrow Asc^{\bullet-} + e^- + H^+$	−0.01
$[Ru^{II}(bpy)_2(bpyNO^{\bullet-})]^{1+} \rightarrow [Ru^{II}(bpy)_2(bpyNO)]^{2+} + e^-$	−1.39
$[Ru^{II}(bpy)_2(H_2O)(bpyNO^{\bullet}H_{out})]^{2+} \rightarrow [Ru^{II}(bpy)_2(H_2O)(bpyNO_{out})]^{2+} + e^- + H^+$	−1.45
$[Ru^{II}(bpy)_2(bpyNO)]^{2+} \rightarrow [Ru^{III}(bpy)_2(bpyNO)]^{3+} + e^-$	+1.00
$[Ru^{III}(bpy)_2(bpyNO)]^{3+} \rightarrow [Ru^{IV}(bpy)_2(bpyNO)]^{3+} + e^-$	+2.88
$[Ru^{II}(bpy)_3]^{2+} \rightarrow [Ru^{III}(bpy)_3]^{3+} + e^-$	+1.29 (1.27)[47]
$[Ru^{I}(bpy)_3]^{1+} \rightarrow [Ru^{II}(bpy)_3]^{2+} + e^-$	−1.71 (−1.31)[47]

[a]The values in the parentheses are from the experiment.

to $[Ru^{IV}(bpy)_2(bpyNO)]^{4+}$ is thermodynamically prohibitive (Table 1). The reduction is ligand-centered and produces the $bpyNO^{\bullet-}$ ligand. A closed configuration, where $bpyNO^{\bullet-}$ is a bidentate ligand to Ru atom, is a predominant state since the reaction occurs in the dark and earlier data has shown that the closed configuration is thermodynamically more favorable.[15,29] Nevertheless, a possibility of an open configuration should not be excluded. Regardless of the configuration, a reductive potential of the $[Ru^{II}(bpy)_2(bpyNO^{\bullet-})]^{1+}$ species is estimated to be significantly more negative than that for Asc used to generate the unique $[Ru^{II}(bpy)(bpyNO^{\bullet-})]^{1+}$ EPR signal (Table 1). Previously, it was shown that DFT results for the Ru complexes can deviate up to ca. −0.5 eV for the reduction reactions.[30] The calculations presented in Table 1 for the $[Ru^{II}(bpy)_2(bpyNO^{\bullet-})]^{1+}$ and $[Ru^{II}(bpy)_2(H_2O)(bpyNO^{\bullet}H_{out})]^{2+}$ correctly predict the localization of an unpaired electron on the bpyNO ligand. We conducted the DFT calculations for multiple possible configurations of the reduced $[Ru(bpy)(bpyNO)]^{1+}$ species and found that only the $[Ru^{II}(bpy)(bpyNO^{\bullet-})]^{1+}$ and $[Ru^{II}(H_2O)(bpy)(bpyNO^{\bullet}H_{out})]^{2+}$ species were energetically viable and provide reasonable ^{14}N hyperfine splitting (hfs) (Table S1). The EPR signal in Figure 1 resembles the EPR spectrum of Ru^{II} complexes with $NO^{\bullet}$ such as *trans*-$[Ru^{II}Cl(NO^{\bullet})(cyclam)]^+$ with $g_{xx} = 2.03$, $g_{yy} = 1.99$, $g_{zz} = 1.88$, and ^{14}N ($I = 1$), hfs $A_{xx} = 17$ G, $A_{yy} = 32$ G, $A_{zz} = 15$ G,[31] and *trans*-$[Ru^{II}(NO^{\bullet})((CH_3CH_2)_2PCH_2CH_2P(CH_2CH_3)_2)_2Cl]^+$ with $g_{xx} = 2.01$, $g_{yy} = 1.98$, $g_{zz} = 1.88$, hfs $A_{xx} = 18$ G, $A_{yy} = 35$ G, and $A_{zz} = 19$ G.[31] The following redox potentials were reported for other Ru complexes with $[Ru^{II}(NO)(L)_5]^{2+}$ structures, such as *trans*-$[Ru(NO)Cl(cyclam)]^{2+}$ with −0.37 V vs Ag/AgCl,[32] *trans*-$[Ru(NO)Cl(1\text{-}(3\text{-propylammonium})cyclam)]^{3+}$ with −0.34 V vs Ag/AgCl,[33] *trans*-$[Ru(NO)Cl(15aneN_4)]^{2+}$ with −0.28 V vs Ag/AgCl[34] and *fac*-$[Ru(NO)Cl_2(k^3N^4,N^8,N^{11}(1\text{-carboxypropyl})cyclam)]^+$ with −0.39 V vs Ag/AgCl[35] (see Figure S1 for the structures).

Spectroscopic Characterization of the Final Product of Light-Induced (1-NO) Transformation. Previously, our group[15] and others[21] have noted the extreme light sensitivity of (**1-NO**). To gain further insight, light-induced changes were monitored using UV−vis, NMR, and resonance Raman spectroscopy (Figures 2−4). We have compared spectroscopic properties of (**1-NO**) after light irradiation with spectra of (**1**). It was found that the product of (**1-NO**) irradiation resembles (**1**). Irradiation for 30 min was performed using three LED monochromatic light sources at 760, 650, and 530 nm. We recorded absorption spectra of irradiated (**1-NO**) with different irradiation times (Figure S3) and found that 30 min light exposure is sufficient to achieve the end of photo reactivity under the experimental condition. The 760 nm light

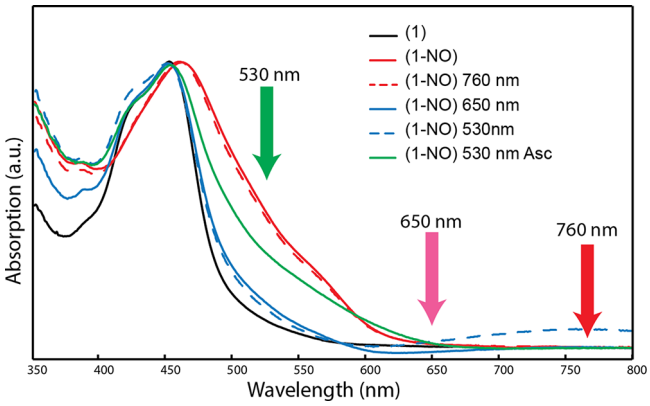

Figure 2. Absorption spectra of 1 mM (**1-NO**) and (**1**) solutions in water (pH 7) before and after irradiation with the different wavelengths (760, 650, and 530 nm) marked by the arrows. The solutions were irradiated for 30 min at a room temperature. To examine the reversibllity, 20 equiv of Acs was added to reduce the sample after the irradiation with the 530 nm LED (dash blue line). Although the small absorption band around 750 nm disappeared upon Asc addition, no absorption maximum shift was observed (green line). The black line is the spectrum of (**1**).

was not effective in changing (**1-NO**) due to low (**1-NO**) absorption at that wavelength. Despite the low absorption at 650 nm, conversion of (**1-NO**) to (**1**) occurs, which shows an extent of (**1-NO**) light sensitivity. As a result of the illumination, the main MLCT peak in (**1-NO**) is blueshifted by about 10 nm to coincide with the main MLCT of (**1**), while the broad peak at ∼560 nm largely disappeared. It was observed that (**1-NO**) transforms to (**1**) by illumination with both 650 and 530 nm light (Figure 2). The deconvolution of UV−vis of the product after 650 nm illumination shows that 70% of (**1-NO**) converted to (**1**), 11% remained intact, and 9% formed other intermediates (Figure S2). In UV−vis absorption spectra, a greater effect was observed under illumination with the 530 nm light. In this case, a new absorption band around 750 nm appeared. This band could be assigned to the Ru^{III} species since the Ru^{III} complexes have an absorption band in the 750 nm region. Asc caused this absorption band to disappear which also supports the assignment of the 750 nm band to the Ru^{III}.

NMR spectroscopy showed evidence of (**1-NO**) to (**1**) conversion (Figure 3). NMR spectrum of (**1**) is well-known[36] and has a distinct signal because of its D_3 point-group symmetry. The majority of the (**1-NO**) converts to (**1**) in D_2O after 30 min of 650 nm illumination (Figure 3). A spectrum after irradiation with the 530 nm light is not shown because the peaks are less resolved due to a presence of paramagnetic

https://dx.doi.org/10.1021/acs.inorgchem.0c01446
Inorg. Chem. XXXX, XXX, XXX−XXX

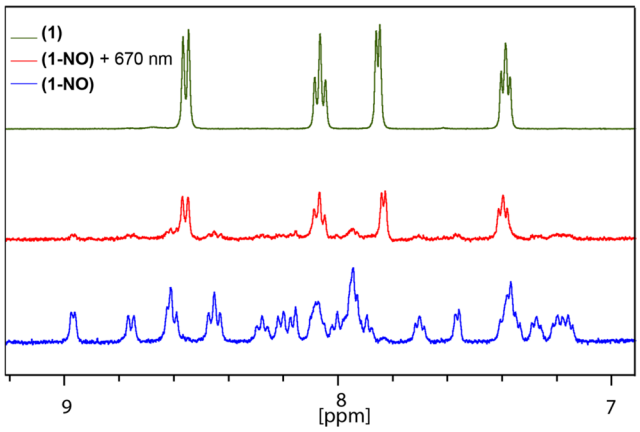

Figure 3. NMR spectra of (**1**), (**1-NO**), and (**1-NO**) illuminated with 650 nm light in D_2O.

Ru^{III} in the reaction mixture. This result is in agreement with the UV−vis spectroscopic data of the Ru^{III} at 530 nm. A presence of the Ru^{III} species was later confirmed by EPR (Figure 5).

Resonance spectroscopy with 442 nm excitation was used to analyze the structural changes in (**1-NO**) (Figure 4). The band

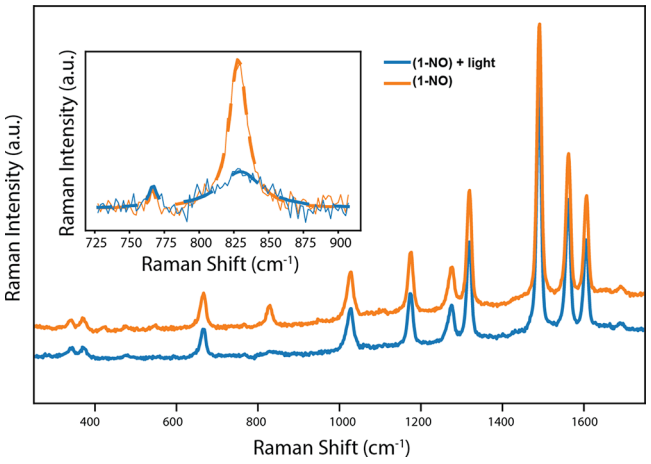

Figure 4. Resonance Raman spectrum of 3 mM solution of (**1-NO**) in water (pH 7) before (orange curve) and after (blue curve) exposure to an ambient light. Spectrum was recorded with 442 nm laser excitation at a room temperature. The measurement took 100 s to minimize the laser damage. The second measurement occurred after 30 min of the ambient light exposure of the sample. The insert is focused on 827 cm^{-1} band and corresponding fits.

at 827 cm^{-1} is typical for the Ru−O−N vibration.[13,15,37] After the illumination all the vibrational bands of (**1-NO**) remain, except the 827 cm^{-1} band, which loses its intensity. In Figure 4 insert, the fitted data show that the intensity of the Ru−N−O band reduced by more than 76%.

EPR studies were used to investigate the paramagnetic intermediates and products of illuminated (**1-NO**). Both Ru^{II} and Ru^{IV} are EPR silent, while Ru^{III} and Ru^{V} are paramagnetic with $S = 1/2$. Ru^{V} complexes with polypyridine ligands are scarce and may also be thermodynamically inaccessible for some complexes.[13,15] The characteristic g-factors of Ru^{V}[37,38] have not been observed in EPR spectra in this study. Light-exposed (**1-NO**) solutions showed formation of at least two coexisting Ru^{III} species. One intermediate has g-factor values of $g_{xx} = 2.64$, $g_{yy} = 2.22$, and $g_{zz} = 1.74$, while the second has $g_{xx} = 2.38$, $g_{yy} = 2.10$, and $g_{zz} = 1.85$ (Figure 5, red and green spectra). We assigned the first one to a Ru^{III} complex with the oxygen atom in bpyNO ligand coordinated to the Ru center ($[Ru^{III}(bpy)_2(bpyNO)]^{3+}$), which is also referred to as the "closed form". Addition of 1 equiv of Ce^{IV} to (**1-NO**) in the dark produces the same signal (Figure 5, black line). The EPR signal of illuminated (**1-NO**) in Figure 5 (green and red spectra) is significantly less intense than (**1-NO**) mixed with 1 equiv of Ce^{IV} (black spectrum), which confirms the UV−vis deconvolution assessment that the majority of illuminated (**1-NO**) is not in the form of Ru^{III}. In addition, a new signal with $g_{xx} = 2.38$, $g_{yy} = 2.10$, and $g_{zz} = 1.85$ was observed and tentatively assigned to a complex with the dissociated ligand such as $[Ru^{III}(H_2O)(bpy)_2(bpyNO_{out})]^{3+}$. g-factors of the Ru^{III} complexes with polipyridine N-oxide ligands reported previously are similar to the g-factors observed in this study.[13,16,37] For example, $g_{xx} = 2.31$, $g_{yy} = 2.2$, and $g_{zz} = 1.91$ have been assigned to oxidized $[Ru^{II}(bpyNO)(tpy)(H_2O)]^{2+}$ compound. Another study[39] on *trans*-$[Ru^{III}(bpy)_2(H_2O)_2]^{3+}$ reported $g_{xx} = 2.38$, $g_{yy} = 2.27$, and $g_{zz} = 1.88$.

Last, to test the (**1-NO**) to (**1**) conversion hypothesis, Ce^{IV} was added to the prolonged-light-exposure (**1-NO**) and compared with Ce^{IV}-oxidized (**1**) (Figure 5, blue and magenta). This comparison indicates that the final products of oxidized illuminated (**1-NO**) and oxidized (**1**) are similar.

Discussion of the Mechanism of the Light-Induced Transformation. Ru polypyridine complexes are well known for their distinct photophysical properties.[40,41] (**1**) and similar Ru-based complexes are among the most-studied systems since they are widely used as photosensitizers.[6,7] Absorption of a photon in (**1**) followed by an intersystem crossing results in a triplet state of (**1**):

$$[Ru^{II}(bpy)_3]^{2+} + h\upsilon \rightarrow [Ru^{II}(bpy)_3]^{2+*} \rightarrow {}^3[Ru^{III}(bpy)_2(bpy^{\cdot-})]^{2+}$$

The lifetime of the charge separated state is solvent-dependent, but on average is ∼1 μs.[42] (**1-NO**) system may undergo similar light excitation and charge separation processes:

$$[Ru^{II}(bpy)_2(bpyNO)]^{2+} + h\upsilon \rightarrow [Ru^{II}(bpy)_2(bpyNO)]^{2+*} \rightarrow {}^3[Ru^{III}(bpy)_2(bpyNO^{-})]^{2+}$$

Figure 6 red arrows represent this path. In (**1**), due to its D_3 point-group symmetry, any of the ligands can be reduced, while for (**1-NO**), the bpyNO ligand becomes reduced due to the higher electronegativity of its N−O moiety. Figure 6 depicts a spin-density distribution for the (**1-NO**) triplet state to illustrate an electron localization on the bpyNO ligand. We compared the well-known photoluminescence of (**1**),[43] (**1-NO**), and (**1-NO**) exposed to light (Figure S4). The intensity of the spectrum is lower in (**1-NO**) compared to (**1**). A ∼4 nm redshift in the emission spectrum of (**1-NO**) indicates the smaller energy band gap between the singlet ground and excited state in (**1-NO**).

As experimental data strongly supports (**1-NO**) to (**1**) conversion, we proposed several viable pathways for this conversion (Figure 6). Since no O_2 evolution was observed for this system under light illumination (Figure S5), the oxygen from the bpyNO ligand would be released either as water or as O•H radical. In Figure 6, one pathway proceeds with the

https://dx.doi.org/10.1021/acs.inorgchem.0c01446
Inorg. Chem. XXXX, XXX, XXX−XXX

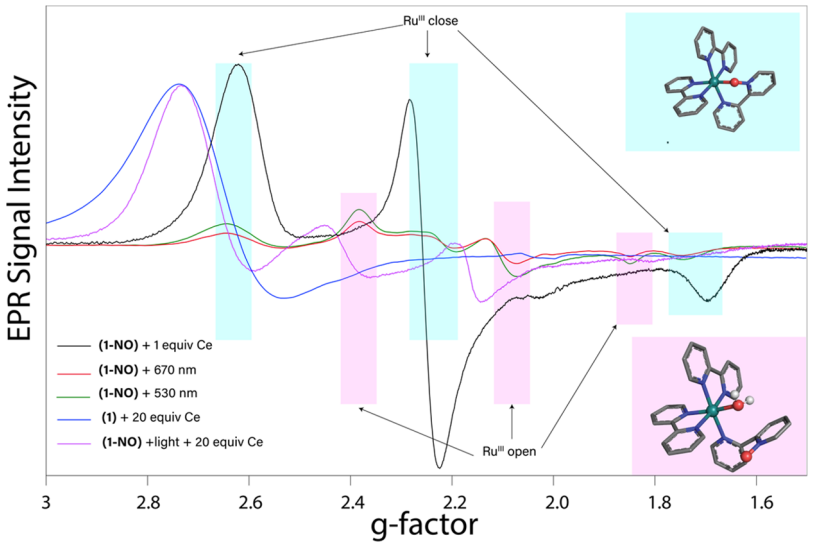

Figure 5. X-band EPR spectra (20 K) of illuminated and oxidized (**1-NO**) and (**1**). Green and red curves represent (**1-NO**) irradiated with 530 and 650 nm light. Black curve is (**1-NO**) oxidized with 1 equiv of Ce^{IV} in the dark. Blue curve is (**1-NO**) oxidized with 20 equiv of Ce^{IV} after an exposure to an ambient light for 3 days. The inserted structures are added to depict a closed and open configuration. pH for Ce^{IV} mixture was 1, and for the rest of samples it was 7.

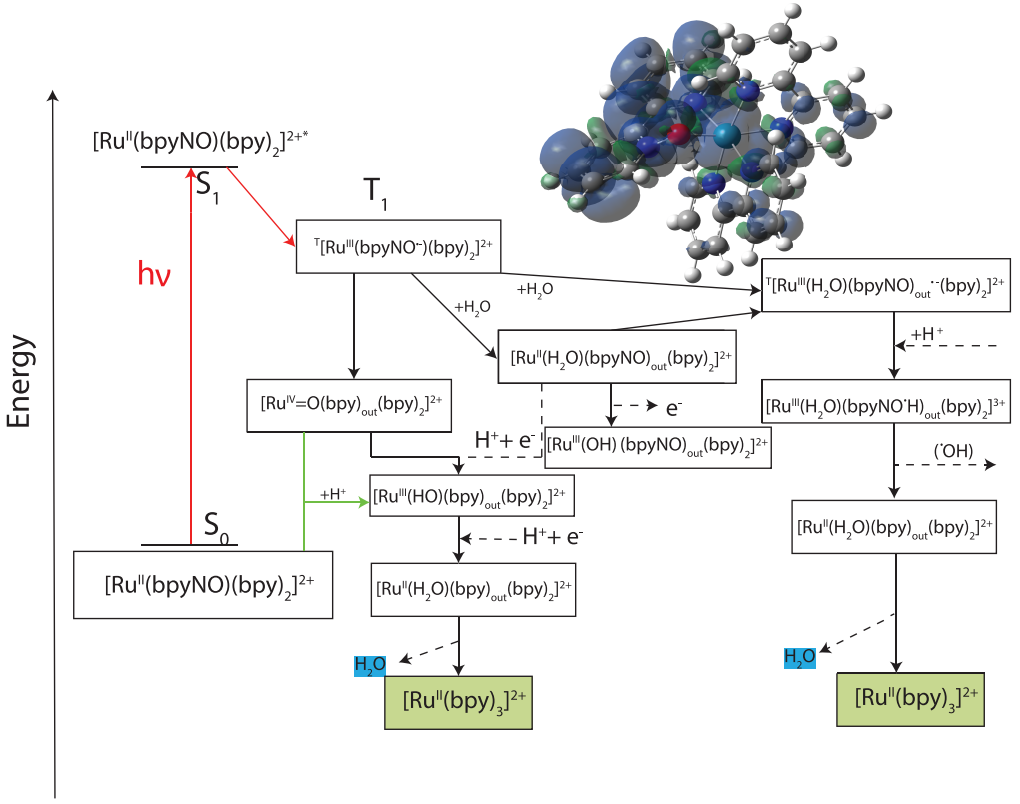

Figure 6. Possible pathways of conversion of (**1-NO**) to (**1**) upon light irradiation. S_0 and S_1 are the singlet ground and excited states, and T_1 is the excited triplet state. The spin density of the triplet state is at the top and shows the electron localization on the bpyNO ligand. The triplet state could transform into two main structures initiating different pathways.

Ru^{IV}═O formation. First, the Ru^{IV} intermediate would be reduced to Ru^{III} followed by conversion to the Ru^{II} species with the release of H_2O. DFT calculations predict a negative free energy for Ru^{IV} to Ru^{III} and Ru^{III} to Ru^{II} reductions. Table 2 presents possible reactions and their corresponding energies. Although this path is thermodynamically favorable, two electrons and protons are needed for its completion. The initial Ru^{II} complex can serve as a reductant to achieve the Ru^{III} state. $[Ru^{III}(bpy)_3]^{3+}$ is known to spontaneously decay in basic solutions with $[Ru^{II}(bpy)_3]^{2+}$ formation.[44] Some literature reports indicate a possibility of a hydroxyl radical production from reduced *N*-oxides via protonation.[45] Decoordinated bpy-*N*-oxide ligand can potentially engage in such a pathway (Figure 6) producing a highly reactive hydroxyl

https://dx.doi.org/10.1021/acs.inorgchem.0c01446
Inorg. Chem. XXXX, XXX, XXX−XXX

Table 2. Calculated Energies of Light-Driven Reactions with DFT[a]

reaction	energy (eV)
$[Ru^{II}(bpyNO)(bpy)_2]^{2+} + h\nu \rightarrow [Ru^{III}(bpyNO^{-\bullet})(bpy)_2]_3^{2+}$	+1.71
$[Ru^{II}(bpyNO)(bpy)_2]^{2+} + h\nu \rightarrow$ 5-coord-$^3[Ru^{II}(bpyNO_{out})(bpy)_2]^{2+}$	+1.69
$^3[RuIII(bpyNO^{-\bullet})(bpy)_2]^{2+} \rightarrow [Ru^{IV}{=}O(bpy)_2(bpy_{out})]^{2+}$	−1.02
$^3[Ru^{III}(bpyNO^{-\bullet})(bpy)_2]^{2+} + H_2O \rightarrow [Ru^{II}(H_2O)(bpy)_2(bpyNO_{out})]^{2+}$	−0.77
$Ru^{II}(bpyNO)(bpy)_2]^{2+} + [Ru^{IV}{=}O(bpy)_2(bpy_{out})]^{2+} + H^+ \rightarrow [Ru^{III}(bpyNO)(bpy)_2]^{3+} + [Ru^{III}(OH)(bpy)_2(bpy_{out})]^{2+}$	+0.04
$[Ru^{II}(bpyNO)(bpy)_2]^{2+} + [Ru^{III}(OH)(bpy)_2(bpy_{out})]^{2+} + H^+ \rightarrow [Ru^{III}(bpyNO)(bpy)_2]^{3+} + [Ru^{II}(H_2O)(bpy)_2(bpy_{out})]^{2+}$	+0.21
$[Ru^{II}(H_2O)(bpy)_2(bpy_{out})]^{2+} \rightarrow [Ru^{II}(bpy)_3]^{2+} + H_2O$	−1.31
$[Ru^{II}(bpyNO)(bpy)_2]^{2+} + [Ru^{IV}{=}O(bpy)_2(bpy_{out})]^{2+} + 2H^+ \rightarrow [Ru^{III}(bpyNO)(bpy)_2]^{3+} + [Ru^{III}(bpy)_3]^{3+} + H_2O$	−0.79
$[Ru^{IV}{=}O(bpy)_2(bpy_{out})]^{2+} + [Ru^{II}(H_2O)(bpy)_2(bpyNO_{out})]^{2+} + H^+ \rightarrow [Ru^{III}(OH)(bpy)_2(bpy_{out})]^{2+} + [Ru^{III}(H_2O)(bpy)_2(bpyNO_{out})]^{3+}$	−0.16
$[Ru^{II}(bpyNO)(bpy)_2]^{2+} + h\nu + H_2O \rightarrow [Ru^{III}(OH)(bpy)_2(bpyNO^{\bullet}H_{out})]^{2+}$	+3.06
$[Ru^{II}(bpyNO)(bpy)_2]^{2+} + h\nu + H^+ \rightarrow$ 5-coord-$[Ru^{III}(bpy)_2(bpyNO^{\bullet}H_{out})]^{2+}$	+2.03

[a]The photon energy is not explicitly entered in the calculations. The energy and coordinates of the complexes can be found in Tables S3 and S4.

radical, which may have potential in the biomedical applications, such as cancer treatments.[8,9,46] However, it is an energetically more demanding pathway (Table 2), and we did not observe any indication of O•H radical formation (data not shown). In both pathways, we assumed that (**1-NO**) is in water solution, where the protons needed for the transformation are readily available. In an attempt to determine the solvent dependency of the (**1-NO**) conversion to (**1**), we illuminated (**1-NO**) dissolved in trifluoroethanol, which is a noncoordinating solvent (Figure S6), although to a lesser extent the conversion still occurs in trifluoroethanol. Another possible pathway that may be solvent independent is oxygen atom transfer from $[Ru^{IV}{=}O(bpy)_2(bpy_{out})]^{2+}$ to the solvent, organic impurities, or bpy ligand with consecutive degradation.

CONCLUSIONS

We have investigated the photochemical and redox behavior of the very light-sensitive (**1-NO**) complex. The bpyNO ligand in (**1-NO**) undergoes a reduction to $bpyNO^{-\bullet}$ in the presence of the mild reducing agent Asc. The UV−vis, NMR, and Raman spectroscopy confirm the formation of (**1**) as a single product of the light irradiation of (**1-NO**). EPR signals observed in the solutions of (**1-NO**) upon the irradiation were assigned to the open and closed forms of the Ru^{III} intermediates. The simulated hfs are in agreement with the EPR measurements and the previous reports of NO radicals coordinated to the Ru center. Several pathways were proposed to explain the conversion of (**1-NO**) to (**1**) and validated with DFT calculations.

ASSOCIATED CONTENT

Supporting Information

The Supporting Information is available free of charge at https://pubs.acs.org/doi/10.1021/acs.inorgchem.0c01446.

Structural formula of the mentioned Ru complexes, absorption spectra of (**1-NO**) and its intermediates, emission spectra, Oxygraph data, DFT summary which includes theoretical energies, hfs, and optimized geometry coordinates (PDF)

AUTHOR INFORMATION

Corresponding Author

Yulia Pushkar − *Department of Physics and Astronomy, Purdue University, West Lafayette, Indiana 47907, United States;* orcid.org/0000-0001-7949-6472; Email: ypushkar@purdue.edu

Authors

Alireza Karbakhsh Ravari − *Department of Physics and Astronomy, Purdue University, West Lafayette, Indiana 47907, United States;* orcid.org/0000-0003-4273-5673

Yuliana Pineda-Galvan − *Department of Physics and Astronomy, Purdue University, West Lafayette, Indiana 47907, United States*

Alexander Huynh − *Department of Physics and Astronomy, Purdue University, West Lafayette, Indiana 47907, United States*

Roman Ezhov − *Department of Physics and Astronomy, Purdue University, West Lafayette, Indiana 47907, United States;* orcid.org/0000-0001-6806-4033

Complete contact information is available at: https://pubs.acs.org/10.1021/acs.inorgchem.0c01446

Funding

This work was supported by the National Science Foundation, Division of Chemistry CHE-1900476 (Y.P.)

Notes

The authors declare no competing financial interest.

ACKNOWLEDGMENTS

Access to EPR was provided by the Amy Instrumentation Facility, Department of Chemistry, Purdue University, under the supervision of Dr. Michael Everly.

REFERENCES

(1) Concepcion, J. J.; Jurss, J. W.; Norris, M. R.; Chen, Z.; Templeton, J. L.; Meyer, T. J. Catalytic Water Oxidation by Single-Site Ruthenium Catalysts. *Inorg. Chem.* **2010**, *49* (4), 1277−1279.

(2) Boddien, A.; Loges, B.; Junge, H.; Gärtner, F.; Noyes, J. R.; Beller, M. Continuous Hydrogen Generation from Formic Acid: Highly Active and Stable Ruthenium Catalysts. *Adv. Synth. Catal.* **2009**, *351* (14−15), 2517−2520.

(3) Zhang, S. Y.; Ding, Y. B.; Wei, H. Ruthenium Polypyridine Complexes Combined with Oligonucleotides for Bioanalysis: A Review. *Molecules* **2014**, *19* (8), 11933−11987.

(4) Grubbs, R. H. Olefin metathesis. *Tetrahedron* **2004**, *60* (34), 7117−7140.

(5) Iglesia, E.; Soled, S. L.; Fiato, R. A. Fischer-Tropsch Synthesis on Cobalt and Ruthenium - Metal Dispersion and Support Effects on Reaction-Rate and Selectivity. *J. Catal.* **1992**, *137* (1), 212−224.

(6) Juris, A.; Balzani, V.; Belser, P.; von Zelewsky, A. Characterization of the Excited State Properties of Some New Photosensitizers of the Ruthenium (Polypyridine) Family. *Helv. Chim. Acta* **1981**, *64* (7), 2175−2182.

(7) O'Regan, B.; Grätzel, M. A low-cost, high-efficiency solar cell based on dye-sensitized colloidal TiO2 films. *Nature* **1991**, *353* (6346), 737−740.
(8) Antonarakis, E. S.; Emadi, A. Ruthenium-based chemotherapeutics: are they ready for prime time? *Cancer Chemother. Pharmacol.* **2010**, *66* (1), 1−9.
(9) Bergamo, A.; Gaiddon, C.; Schellens, J. H. M.; Beijnen, J. H.; Sava, G. Approaching tumour therapy beyond platinum drugs: Status of the art and perspectives of ruthenium drug candidates. *J. Inorg. Biochem.* **2012**, *106* (1), 90−99.
(10) Meyer, T. J.; Huynh, M. H. The remarkable reactivity of high oxidation state ruthenium and osmium polypyridyl complexes. *Inorg. Chem.* **2003**, *42* (25), 8140−60.
(11) Kamdar, J. M.; Grotjahn, D. B. An Overview of Significant Achievements in Ruthenium-Based Molecular Water Oxidation Catalysis. *Molecules* **2019**, *24* (3), 494.
(12) Zhang, B.; Sun, L. Artificial photosynthesis: opportunities and challenges of molecular catalysts. *Chem. Soc. Rev.* **2019**, *48* (7), 2216−2264.
(13) Ravari, A. K.; Zhu, G.; Ezhov, R.; Pineda-Galvan, Y.; Page, A.; Weinschenk, W.; Yan, L.; Pushkar, Y. Unraveling the Mechanism of Catalytic Water Oxidation via de Novo Synthesis of Reactive Intermediate. *J. Am. Chem. Soc.* **2020**, *142* (2), 884−893.
(14) Pineda-Galvan, Y.; Ravari, A. K.; Shmakov, S.; Lifshits, L.; Kaveevivitchai, N.; Thummel, R.; Pushkar, Y. Detection of the site protected 7-coordinate RuV = O species and its chemical reactivity to enable catalytic water oxidation. *J. Catal.* **2019**, *375*, 1−7.
(15) Pushkar, Y.; Pineda-Galvan, Y.; Ravari, A. K.; Otroshchenko, T.; Hartzler, D. A. Mechanism for O-O bond formation via radical coupling of metal and ligand based radicals − a new pathway. *J. Am. Chem. Soc.* **2018**, *140* (42), 13538−13541.
(16) Moonshiram, D.; Pineda-Galvan, Y.; Erdman, D.; Palenik, M.; Zong, R. F.; Thummel, R.; Pushkar, Y. Uncovering the Role of Oxygen Atom Transfer in Ru-Based Catalytic Water Oxidation. *J. Am. Chem. Soc.* **2016**, *138* (48), 15605−15616.
(17) Mfuh, A. M.; Larionov, O. V. Heterocyclic N-Oxides - An Emerging Class of Therapeutic Agents. *Curr. Med. Chem.* **2015**, *22* (24), 2819−2857.
(18) Li, D. L.; Wu, P. P.; Sun, N.; Lu, Y. J.; Wong, L.; Fang, Z. Y. A.; Zhang, K. The Diversity of Heterocyclic N-oxide Molecules: Highlights on their Potential in Organic Synthesis, Catalysis and Drug Applications. *Curr. Org. Chem.* **2019**, *23* (5), 616−627.
(19) Kojima, T.; Nakayama, K.; Sakaguchi, M.; Ogura, T.; Ohkubo, K.; Fukuzumi, S. Photochemical Activation of Ruthenium(II)-Pyridylamine Complexes Having a Pyridine-N-Oxide Pendant toward Oxygenation of Organic Substrates. *J. Am. Chem. Soc.* **2011**, *133* (44), 17901−17911.
(20) Petrosyan, A.; Hauptmann, R.; Pospech, J. Heteroarene N-Oxides as Oxygen Source in Organic Reactions. *Eur. J. Org. Chem.* **2018**, *2018* (38), 5237−5252.
(21) Ghosh, P. K.; Brunschwig, B. S.; Chou, M.; Creutz, C.; Sutin, N. Thermal and Light-Induced Reduction of Ru(bpy)3(3+) in Aqueous-Solution. *J. Am. Chem. Soc.* **1984**, *106* (17), 4772−4783.
(22) Kalyanasundaram, K. Photophysics, photochemistry and solar energy conversion with tris(bipyridyl)ruthenium(II) and its analogues. *Coord. Chem. Rev.* **1982**, *46*, 159−244.
(23) Teply, F. Photoredox Catalysis by Ru(bpy)(3) (2+) to Trigger Transformations of Organic Molecules. Organic Synthesis Using Visible-Light Photocatalysis and Its 20th Century Roots. *Collect. Czech. Chem. Commun.* **2011**, *76* (7), 859−917.
(24) Young, K. J.; Martini, L. A.; Milot, R. L.; Snoeberger, R. C.; Batista, V. S.; Schmuttenmaer, C. A.; Crabtree, R. H.; Brudvig, G. W. Light-driven water oxidation for solar fuels. *Coord. Chem. Rev.* **2012**, *256* (21−22), 2503−2520.
(25) Zhang, S. F.; Yang, X. D.; Numata, Y. H.; Han, L. Y. Highly efficient dye-sensitized solar cells: progress and future challenges. *Energy Environ. Sci.* **2013**, *6* (5), 1443−1464.
(26) Motten, A. G.; Hanck, K.; DeArmound, M. K. ESR of the reduction products of [Fe(bpy)3]2+ and [Ru(bpy)3]2+. *Chem. Phys. Lett.* **1981**, *79* (3), 541−546.
(27) Warren, J. J.; Mayer, J. M. Tuning of the Thermochemical and Kinetic Properties of Ascorbate by Its Local Environment: Solution Chemistry and Biochemical Implications. *J. Am. Chem. Soc.* **2010**, *132* (22), 7784−7793.
(28) Miyazaki, H.; Matsuhisa, Y.; Kubota, T. Cyclic Voltammetry of Aromatic Amine N-Oxides in Non-aqueous Solvents and the Stability of the Free-Radicals Produced. *Bull. Chem. Soc. Jpn.* **1981**, *54* (12), 3850−3853.
(29) Govindarajan, N.; Meijer, E. J. Modeling the Catalyst Activation Step in a Metal-Ligand Radical Mechanism Based Water Oxidation System. *Inorganics* **2019**, *7* (5), 62.
(30) Baik, M.-H.; Friesner, R. A. Computing Redox Potentials in Solution: Density Functional Theory as A Tool for Rational Design of Redox Agents. *J. Phys. Chem. A* **2002**, *106* (32), 7407−7412.
(31) McGarvey, B. R.; Ferro, A. A.; Tfouni, E.; Bezerra, C. W. B.; Bagatin, I.; Franco, D. W. Detection of the EPR spectra of NO center dot in ruthenium(II) complexes. *Inorg. Chem.* **2000**, *39* (16), 3577−3581.
(32) Lang, D. R.; Davis, J. A.; Lopes, L. G. F.; Ferro, A. A.; Vasconcellos, L. C. G.; Franco, D. W.; Tfouni, E.; Wieraszko, A.; Clarke, M. J. A Controlled NO-Releasing Compound: Synthesis, Molecular Structure, Spectroscopy, Electrochemistry, and Chemical Reactivity of R,R,S,S-trans-[RuCl(NO)(cyclam)]2+(1,4,8,11-tetraazacyclotetradecane). *Inorg. Chem.* **2000**, *39* (11), 2294−2300.
(33) Ferreira, K. Q.; Doro, F. G.; Tfouni, E. Aquation reactions of RuII and RuIII dichloro complexes with 1-(3-propylammonium)-cyclam: Properties of trans-[RuClL(1-(3-propylammonium)cyclam)]-n+ complexes (L═Cl−, tfms−, H2O). *Inorg. Chim. Acta* **2003**, *355*, 205−212.
(34) Oliveira, F. d. S.; Togniolo, V.; Pupo, T. T.; Tedesco, A. C.; da Silva, R. S. Nitrosyl ruthenium complex as nitric oxide delivery agent: synthesis, characterization and photochemical properties. *Inorg. Chem. Commun.* **2004**, *7* (2), 160−164.
(35) Doro, F. G.; Pepe, I. M.; Galembeck, S. E.; Carlos, R. M.; da Rocha, Z. N.; Bertotti, M.; Tfouni, E. Reactivity, photolability, and computational studies of the ruthenium nitrosyl complex with a substituted cyclam fac-[Ru(NO)Cl2(κ3N4,N8,N11(1-carboxypropyl)cyclam)]Cl·H2O. *Dalton Trans.* **2011**, *40* (24), 6420−6432.
(36) Iranmanesh, H.; Bhadbhade, M.; De Haas, N.; Luis, E. T.; Yan, H.; Yang, J.; Beves, J. E. Badly behaving bipyridine: the surprising coordination behaviour of 5,5′-substituted-2,2′-bipyridine towards iron(II) and ruthenium(II) ions. *Supramol. Chem.* **2015**, *27* (11−12), 854−864.
(37) Pineda-Galvan, Y.; Ravari, A. K.; Shmakov, S.; Lifshits, L.; Kaveevivitchai, N.; Thummel, R.; Pushkar, Y. Detection of the site protected 7-coordinate Ru-V = O species and its chemical reactivity to enable catalytic water oxidation. *J. Catal.* **2019**, *375*, 1−7.
(38) Dengel, A. C.; Griffith, W. P. Studies on transition-metal oxo and nitrido complexes. 12. Synthesis, spectroscopic properties, and reactions of stable ruthenium(V) and osmium(V) oxo complexes containing.alpha.-hydroxy carboxylate and.alpha.-amino carboxylate ligands. *Inorg. Chem.* **1991**, *30* (4), 869−871.
(39) Planas, N.; Vigara, L.; Cady, C.; Miró, P.; Huang, P.; Hammarström, L.; Styring, S.; Leidel, N.; Dau, H.; Haumann, M.; Gagliardi, L.; Cramer, C. J.; Llobet, A. Electronic Structure of Oxidized Complexes Derived from cis-[RuII(bpy)2(H2O)2]2+ and Its Photoisomerization Mechanism. *Inorg. Chem.* **2011**, *50* (21), 11134−11142.
(40) Anderson, C. P.; Salmon, D. J.; Meyer, T. J.; Young, R. C. Photochemical Generation of Ru(bpy)3+ and 02. *J. Am. Chem. Soc.* **1977**, *99* (6), 1980−1982.
(41) Caspar, J. V.; Meyer, T. J. Photochemistry of tris(2,2′-bipyridine)ruthenium(2+) ion (Ru(bpy)32+). Solvent effects. *J. Am. Chem. Soc.* **1983**, *105* (17), 5583−5590.

https://dx.doi.org/10.1021/acs.inorgchem.0c01446
Inorg. Chem. XXXX, XXX, XXX−XXX

(42) Kaizu, Y.; Ohta, H.; Kobayashi, K.; Kobayashi, H.; Takuma, K.; Matsuo, T. Lifetimes of the lowest excited state of tris(2,2′-bipyridine)ruthenium(II) and its amphipathic derivative in micellar systems. *J. Photochem.* **1985**, *30* (1), 93−103.
(43) Ogawa, M.; Kuroda, K. Photofunctions of Intercalation Compounds. *Chem. Rev.* **1995**, *95* (2), 399−438.
(44) Singh, W. M.; Pegram, D.; Duan, H.; Kalita, D.; Simone, P.; Emmert, G. L.; Zhao, X. Hydrogen Production Coupled to Hydrocarbon Oxygenation from Photocatalytic Water Splitting. *Angew. Chem., Int. Ed.* **2012**, *51* (7), 1653−1656.
(45) Konev, M. O.; Cardinale, L.; Jacobi von Wangelin, A. Catalyst-Free N-Deoxygenation by Photoexcitation of Hantzsch Ester. *Org. Lett.* **2020**, *22* (4), 1316−1320.
(46) Nakanishi, I.; Nishizawa, C.; Ohkubo, K.; Takeshita, K.; Suzuki, K. T.; Ozawa, T.; Hecht, S. M.; Tanno, M.; Sueyoshi, S.; Miyata, N.; Okuda, H.; Fukuzumi, S.; Ikota, N.; Fukuhara, K. Hydroxyl radical generation via photoreduction of a simple pyridine N-oxide by an NADH analogue. *Org. Biomol. Chem.* **2005**, *3* (18), 3263−3265.
(47) Rillema, D. P.; Allen, G.; Meyer, T. J.; Conrad, D. Redox properties of ruthenium(II) tris chelate complexes containing the ligands 2,2′-bipyrazine, 2,2′-bipyridine, and 2,2′-bipyrimidine. *Inorg. Chem.* **1983**, *22* (11), 1617−1622.

https://dx.doi.org/10.1021/acs.inorgchem.0c01446
Inorg. Chem. XXXX, XXX, XXX−XXX